Available online at www.HighTechJournal.org

HighTech and Innovation Journal

ISSN: 2723-9535

Vol. 5, No. 4, December, 2024

Improving Sensing Measurements Using Laser Self-Mixing Interference in Non-Line-of-Sight Optical Communication via Systems

Sichen Lu [1*], Changying Guo [2*]

[1] *Department of Computer and Information Science, College of Bardon Jilin Normal University, Siping, 136523, China.*

[2] *State Grid Gansu Electric Power Research Institute, Lanzhou 730070, China.*

Received 21 February 2024; Revised 30 October 2024; Accepted 06 November 2024; Published 01 December 2024

Abstract

Objective: Mobile robots leverage laser self-mixing interference for sensing in non-line-of-sight optical communications, allowing for a wide range of measures such as distance, velocity, and displacement, while also improving accuracy and flexibility in robotic navigation and interaction. Interference, restricted range, and sensitivity to environmental factors are challenges that affect the precision and reliability of sensing measures. *Methods:* This paper presents a detailed introduction to theory and various algorithms of channel estimation in wireless communication. Combining the characteristics of UV channels, a channel estimation algorithm suitable for UV optical communication systems is selected, and relevant simulations are carried out. A theoretical analysis of channel estimation SNR and a proposed angle measurement method using laser self-mixing interference are discussed. A device is designed to implement this method, utilizing self-mixing interferometric fringe counting to measure rotation displacement in mobile robots. *Findings:* In results, sensing measurement and modality are employed for SNR and robotic localization performance. Distance (15 dB), velocity (12 dB), and object shape (18 dB) in SNR and laser range finder (5 cm), camera (15 cm), and LiDAR (3 cm) in robotic localization performance. *Conclusion:* Incorporating laser self-mixing interference effects into non-line-of-sight optical communication for mobile robotics enhances sensing precision across diverse measurements, fostering robustness and adaptability in dynamic environments.

Keywords: Mobile Robots; Displacement Measurement; Non-Line-of-Sight Optical Communication Signal Processing; Systems, Channel Estimation; Optical Feedback Self-Mixing Interference; Angle Measurement.

1. Introduction

Since the 1960s, the research and application of mobile robots abroad have developed to a new stage, and significant breakthroughs have been made in technology and products [1]. At present, the main research results at home and abroad include the modeling of robotic systems [2]. The first is to describe the complex motion state by building a model, and the second is to determine what needs to be done for each task and how to achieve these functions according to different task requirements [3]. Finally, computers are used to simulate the various parameters that exist in the real environment in order to develop strategies and to solve and investigate path planning problems [4]. The application of sensors is the most important and representative issue in the field of mobile robotics, so a deeper, multi-faceted, and comprehensive design and analysis of mobile robot sensing and measurement is required. The real-life environment is complex and unpredictable, and external factors are diverse and unpredictable [5, 6]. In order to better serve the robot and achieve its

* Corresponding author: gcyzwt@nyist.edu.cn; bdjsj_lsc@163.com

http://dx.doi.org/10.28991/HIJ-2024-05-04-012

intelligent movement goals, we need to take into account a wide range of situations: the type of sensor and the range of sensor sensing areas.

The basic principle of UV light communication is that the frequency signal generated by a modulator can be used to drive a light wave in an optical fiber. Due to the fast propagation speed and large bandwidth of UV light, different levels and types of FM amplification circuits can be used to perform multi-stage switching functions. The filtering section is used to eliminate system noise and minimize interference. Uses filters such as low-pass filters and band-pass filters [7-9]. This paper summarizes and studies the latest UV atmospheric transmission characteristics, as well as the UV communication channel model and impulse response, and uses an adaptive channel estimation algorithm for the first time in the UV communication system to achieve the estimation of the UV channel. To improve the overall communication performance of the UV optical communication system. Achieving high-speed, reliable data communication transmission in UV-optical communication is a key step in the use of UV-optical communication for networking as well as for video transmission in military communications [10-12]. Theoretical studies have shown that the channel capacity of UV optical communication systems is between 100kb and 400kb in the non-visual range case. MIMO techniques and space-time coding techniques can increase channel capacity and combat fading effects due to various causes. In addition, theoretical analyses have shown that multiple input and multiple output in ultraviolet optical communication is also an effective means of increasing transmission rates [13].

Laser interferometry is a non-contact measurement method that is widely used in industry and has attracted a lot of attention from scholars at home and abroad due to its promising development and broad applications [14]. Interference is achieved by compressing an optical pulse and using the laser beam to interact with different materials. The principle is that when the light source emits high frequency energy, a single photon center and multiple vibrational centers are formed due to a large number of electron-hole complex effects within the atom, which also lead to the existence of other defects such as dipoles (or dipoles) between two vibrational surfaces or mutual attraction between excited states, resulting in a change of spatial phase [15, 16].

Non-Line-of-Sight imaging system is a technique for reconstructing an object which isn't in the camera's direct line of sight by utilizing light dispersed between one or multiple surfaces around the occluded objects. This light is reflected and scattered numerous times before reaching the detector or the camera, producing in a lower ratio of signal-to-noise [17]. Mobile robots use Non-Line-of-Sight optical Communication Signal Processing for navigating difficult surroundings. Through examining the reflections of light and shadows, robots determine its environment by interpreting obscured signals. This technique allows robots to perform efficiently even if direct communication lines are blocked, increasing autonomy and flexibility.

Laser self-mixing interference happens whenever a part of the light generated through a laser gets reflected by an external target, and entering into the laser's active cavity again. As a consequence, the frequency and amplitude associated with the lasers oscillating fields are modulated [18]. Laser self-mixing interference uses feedback within laser diodes for detect displacement, vibration, velocity, and other characteristics. It provides the cost-effectiveness, compactness, and higher sensitivity which makes it useful for a wide range of applications, including biomedical sensing, automotive navigation, and industrial metrology. Its adaptability continuing driving sensing technology innovations.

The main goal of this paper is to develop efficient signal processing algorithms for mobile robotics, utilizing laser self-mixing interference in non-line-of-sight optical communication, optimizing sensing measurements across diverse environments.

The remainder of this research is organized in the following manner: The literature review are presented in section 2. Non-Line-of-sight optical communications are explained in section 3. Building an ultraviolet optical communication channel estimation system for mobile robots are described in section 4. Construction of a laser self-mixing interferometric angle measurement device for mobile robots are determined in section 5. The results are presented in section 6. Conclusion are presented in section 7.

2. Literature Review

Sun et al. [19] presented a technique that uses repeated self-mixing interference using absorption to detect the indicator Fe^{2+} within electrolyte samples containing a micro molar concentration. Liu et al. [20] provided an enhanced wavelet thresholds denoising technique of laser self-mixing interference signaling. Wang et al. [21] explained a novel signal processing approach has been developed called orthogonal signal phase multiplication. It is utilized to increase the accuracy of vibration measurements within a phase modulating self-mixing interferometers. Yu et al. [22] developed

an acoustic emission (AE) detecting sensors that combines optical fiber sensors using laser self-mixing interference technique. Shen et al. [23] created a new area of wireless sensing that had been used in posture identification, object location, as well as additional sensing applications based on the RFID technology. As the RFID-based framework becomes operational, the signal experiences substantial alterations as an object travel between two or more various Fresnel regions. Liu et al. [24] generated a period-multiplexed fiber-coupled laser self-mixing interferometry sensors that uses an impulsive excitation approach to measure materials' shear modulus, the Poisson's ratio, and the young modulus at the same time. Zhao & Zhang [25] provided an angle measuring technique depending on speckle-affected self-mixing interference signals. Higher and lower frequencies noises within the SMI signals could be concurrently filtered out through variable modes decomposition.

2.1. Research gap

This paper addresses challenges in mobile robot sensing using laser self-mixing interference. It introduces a UV optical communication channel estimation algorithm, conducts simulations, and analyzes signal-to-noise ratio. Additionally, it proposes an angle measurement method based on self-mixing interference and designs a device for implementation, enhancing robotic navigation precision.

3. Non-Line-of-Sight Optical Communications System

3.1. Single Scattering Model for UV Non-Line-of-Sight Optical Communication

Figure 1 represents the communication link diagram for non-visible UV scattering.

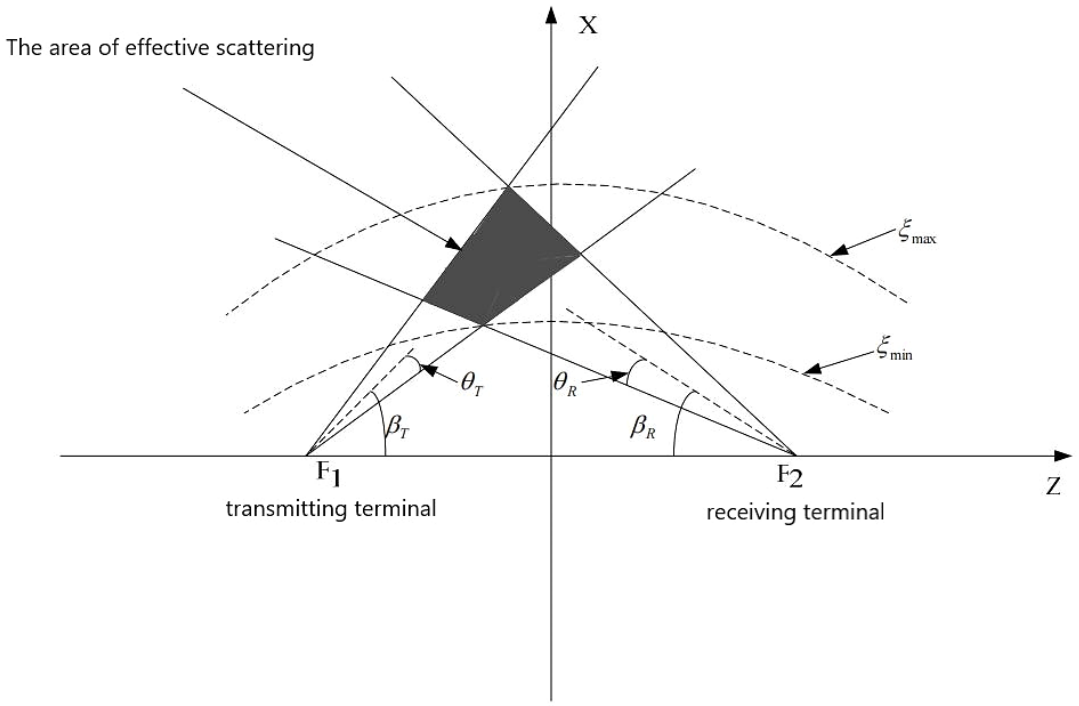

Figure 1. Communication link diagram for non-visible UV scattering

The transmitter is placed at focus F1 and the receiver at focus F2, and it is assumed that the cone axes of the transmitting beam and the receiving field of view lie in the same plane. In Figure 1, their axes are both located in the x-z plane. The single scattering model is based on the idea that photons are only scattered once by the atmosphere during their entire transmission from emission to reception. The scattering process occurs randomly and it is possible to produce two or more scattering interactions, the magnitude of the probability of which is related to the geometrical position between the emitter and receiver and the atmospheric properties. When r is less than or equal to 1.0, the single scattering model is a reasonable modelling of the actual system, and the UV non-visual communication system is a short-range scattering communication that satisfies this condition. The following calculates the relationship between the energy and the time received at the receiving end as a function of single scattering when a pulse is emitted [26]. Consider a pulse with energy $Q_T$emitted at $t = 0$. Let the energy be uniformly distributed in the emitting cone, and the energy per unit's area of point p at distance r1 from the emitting point as:

$$H_P = \frac{Q_T \exp(-k_e r_1)}{\Omega_T (r_1)^2}, t = \frac{r_1}{c} \tag{1}$$

where Q_T represent the impulse transmitter energy at $t = 0$, k_e indicates the atmospheric coefficient of extinction, Ω_T signifies the energy impulse, r demonstrates the inter focal distance, t is the time, and c is the light speed.

A volume element containing a point *P* could be considered as a radiation secondary source, radiating a total energy to the whole space of:

$$\delta Q_P = k_s H_P \delta V = k_s \frac{Q_T \exp(-k_e r_1)}{\Omega_T (r_1)^2} \delta V \tag{2}$$

where the coefficient of atmospheric scatter is k_s, δVrepresents the differential volume.

The scattering in all directions is not equal, and the scattered energy per units of steradian angle in the direction of the scattering angle and the scattered energy per unit's of area received on the receiving end of this secondary source is

$$\delta R_P = \frac{\delta Q_P P(\theta_s)}{4\pi} \tag{3}$$

where $P(\theta_s)$ signifies the single-scatter phase functioning.

$$\delta H_R = \frac{\delta R_p \cos(\zeta) \exp(-k_e r_2)}{r_2^2} = \frac{Q_T k_s \cos(\zeta) \exp(-k_e (r_1 + r_2))}{4\pi \Omega_T (r_1 r_2)^2} P(\theta_s) \delta V \tag{4}$$

where ζ is denotes an angle between the axis of the receiver and a vectors pointing from their receiver to its volume elements.

In the long spherical coordinate system, the volume element can be expressed as:

$$\delta V = \frac{r^3}{8} (\xi^2 - \eta^2) \delta\xi \delta\eta \delta\varphi \tag{5}$$

In summary, it follows that the energy per unit area received is:

$$\frac{\delta H_R}{\delta t} = \frac{Q_T c k_s \cos(\zeta) \exp(-k_s r \xi)}{2\pi \Omega_T r (\xi^2 - \eta^2)} P(\theta_s) \delta\eta \delta\varphi \tag{6}$$

$$\delta E(\xi) = \frac{\delta H_R}{\delta t} \tag{7}$$

The received radiance is obtained by substituting equation 7 into the above equation and integrating over the entire determined long sphere. Alternatively, the inherent cone angle of the transmitter is:

$$\Omega_T = 4\pi \sin^2\left(\frac{\theta_T}{2}\right) \tag{8}$$

where θ_T indicates the divergence of the beam transmitter.

The energy is uniformly distributed over this cone angle range and the received irradiance is further obtained from Equation 9 and the total energy received is Equation 12:

$$E(\xi) = \begin{cases} 0 & (\xi < \xi_{min}) \\ \frac{Q_r c k_s \exp(-k_e r \xi)}{2\pi \Omega_r r^2} \int_{\eta_0(\xi)}^{\eta_2(\xi)} \frac{2g[\varphi_2(\xi,\eta)]}{(\xi^2 - \eta^2)} P(\theta_s) d\eta & (\xi_{min} \le \xi \le \xi_{max}) \\ 0 & (\xi < \xi_{max}) \end{cases} \tag{9}$$

$$\cos(\zeta) = \cos(\beta_R)\cos(\Psi_1) + \sin(\beta_R)\sin(\Psi_1)\cos(\varphi) \tag{10}$$

where β_R represents the apex receiver angle.

$$g[\varphi_2(\xi,\eta)] = \varphi_2(\xi,\eta)\cos\beta_R \cos\Psi_1 + \sin\beta_R \sin\Psi_1 \sin\varphi_2(\xi,\eta) \tag{11}$$

$$E_R = \int_{t_{min}}^{t_{max}} E\left(c\frac{t}{r}\right) dt \tag{12}$$

The product of the energy emitted by the transmitter after attenuation and the energy after scattering is integrated over the time range to obtain the total energy detected by the detector, and the resulting E(t) is the impulse response of the channel. The limits of integration for angular and azimuthal coordinates are respectively.

$$\eta_1(\xi) = \max\{\eta_{1,R}, \eta_{1,T}\}(\xi_{\min} \le \xi \le \xi_{\max}) \quad (13)$$

$$\eta_2(\xi) = \min\{\eta_{2,R}, \eta_{2,T}\}(\xi_{\min} \le \xi \le \xi_{\max}) \quad (14)$$

$$\varphi_2(\xi, \eta) = \min\{\varphi_{2,R}(\xi, \eta), \varphi_{2,T}(\xi, \eta)\} \quad (15)$$

After analysis, it is found that the angular coordinate is a monotonic function of the azimuthal coordinate, and when the azimuthal coordinate is small, the channel response is in the primary stage, and the impulse response of the channel can be obtained by simplifying the integral limits obtained at this time.

$$h(t) = \frac{const^* k_s \exp(-k_e ct)}{16\pi^2 r \sin^2(\theta_T/2)} \times \frac{1}{t} \times \{\ln(c^2t^2 - 2crcos(\beta_R - \theta_R)t + r^2]\} - \ln\{[c^2t^2 - 2crcos(\beta_T - \theta_T)t + r^2]\} \quad (16)$$

Where θ_R represents the receiver's half-field of view, and β_T indicates the apex transmitter angle.

3.2. Theory of Channel Estimation for UV Optical Communication System

During the scattering and transmission of UV signals in the atmosphere, the light pulse signal is affected by path loss on the one hand, and the pulse spreading effect leads to inter-code interference on the other hand, resulting in a sharp deterioration of the received signal. The various distortions in the received signal have a serious impact on the demodulation and judgement decoding at the back-end. Therefore, it is essential to ensure the integrity of the UV signal during atmospheric transmission and to overcome the effects of inter-code interference at the receiving end as far as possible.

The UV non-line-of-sight communication system is a short-range, low-rate communication system with a narrow communication bandwidth, and a training sequence-based estimation method is used to perform channel estimation for UV non-line-of-sight communication. The frame structure is first designed at the transmitter side by inserting a Barker code and a Gold sequence as the frame synchronisation and training sequence respectively, and then the channel parameters are estimated using a channel estimation algorithm for the received data through the channel estimation module. When the channel characteristics change, the adaptive algorithm follows the channel changes to make a new channel estimate. The new channel parameters are estimated. The channel estimation can be applied in several modules, ultimately allowing the maximum recovery of the received signal [27].

When more reliable channel parameters are obtained, the transmitter can adjust the transmitting strategy to suit the channel. If the modulation and coding are fixed, it is not possible to match the channel to the optimum [28]. Also, the judgement threshold can be set adaptively based on the estimated channel parameters. In UV optical communication, the threshold is not fixed because the noise is signal dependent, and the noise is not yet Gaussian. It is the adaptive judgement threshold that can adapt to the time-varying characteristics of the channel and can be close to the optimal threshold.

1. Design of the frame structure

The purpose of the frame structure on the transmitter side is to synchronise the frames and to prepare the training sequence for channel estimation, using a 13-bit Barker code for frame synchronisation and an m sequence for the training sequence. The frame structure is shown in Figure 2, and at the receiver side the frame synchronisation is extracted as shown in Figure 3.

Figure 2. Frame structure

In digital wireless communication, a certain number of code elements are often combined for transmission, and this collection of data is usually called a frame. Frame synchronisation is often the last and most critical step in system synchronisation and is directly related to the subsequent signal processing. The frame is the basic unit of data transmission and different digital wireless communication systems have different frame structures, which need to be designed according to the specific application. Based on the common frame structure of wireless communication, the frame structure of the UV non-visual communication system has been designed to improve the communication performance. In this paper, the Barker code is inserted to identify the start of the frame. 13-bit Barker code autocorrelation function is shown in Figure 4.

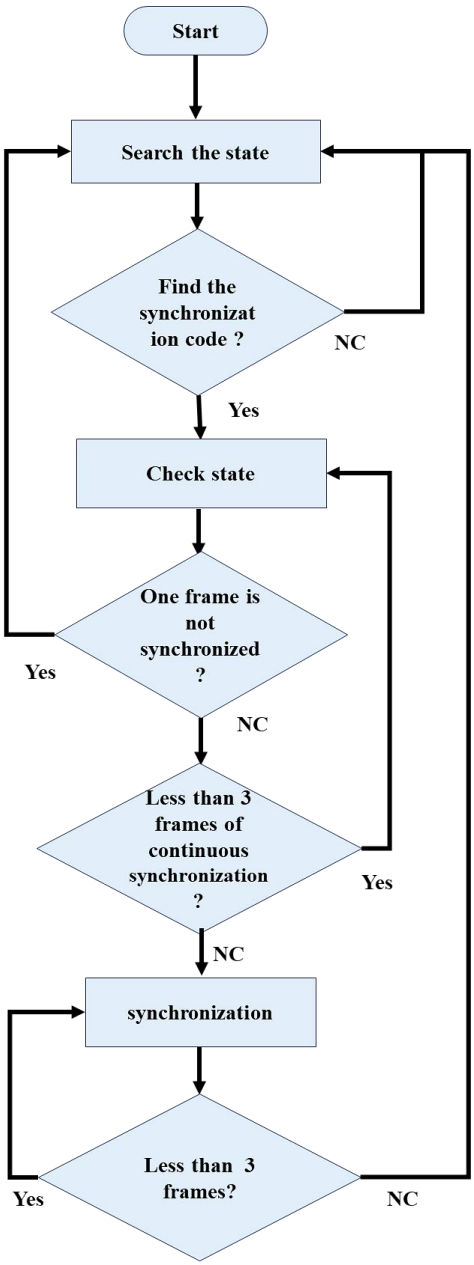

Figure 3. Frame synchronisation jump

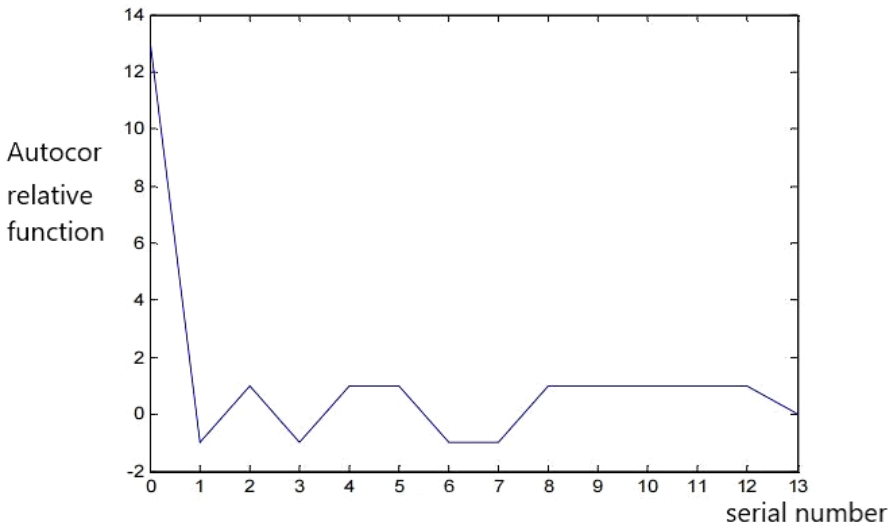

Figure 4. 13-bit Barker code autocorrelation function

The basic method to achieve frame synchronization is to insert a special code type of frame synchronization code set into a pre-defined time slot, i.e., the frame synchronization code time slot, at the transmitter side. At the receiving end, the autocorrelation of the synchronization codes is used to determine the synchronization position of the frame. The frame synchronization code set can be inserted centrally or decentrally.

3.3. Laser Self-Mixing Interferometry Principle

The principle of laser interferometry is that in a high-resolution optical receiver, light waves of different wavelengths are generated by modulation and converted into the same monochromatic or multiple colors. When the light source emits a narrow pulse, the beam is reflected back, and the receiver collects all signals in that band. It can therefore be used to process, analyze, and extract multispectral information using a computer; in addition, it can be used to measure the variation in distance between points in the laser system and the receiver station to obtain the location and angular distribution of the target surface. In this paper, a three-mirror cavity equivalent model is used for analysis, as shown in Figure 5, and the equivalent numerical model is shown in Equations 17 to 19. In this paper, only the propagation of the laser signal in the one-dimensional direction of the three-mirror cavity model is considered, i.e., when r1 is smaller than r2.

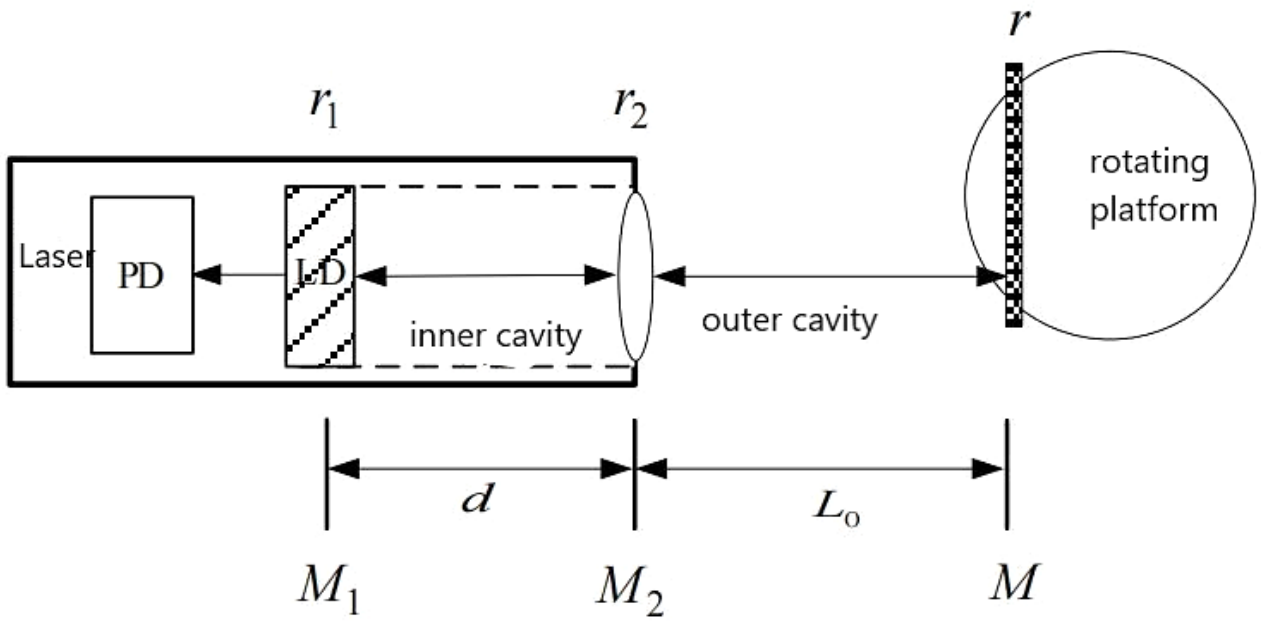

Figure 5. Equivalent model of the three mirror cavities

$$\omega_F\tau = \omega_0\tau - C\sin[\omega_F\tau + \arctan\alpha] \quad (17)$$

$$P(\omega_F\tau) = P_0[1 + mF(\omega_F(\tau)] \quad (18)$$

$$F(\omega_F\tau) = \cos(\omega_F\tau) \quad (19)$$

The equation of the three-mirror cavity equivalent model shows that the generation of self-mixed interference fringes is not only related to the optical feedback level factor, but also to the variation of the line width spreading factor. Therefore, simulations are carried out to verify and analyze the two separately. Figure 6 shows the SMI signal at different optical feedback levels and the SMI signal at different line width spreading levels.

Therefore, for the angular measurement method designed what is required is a stripe at a moderate feedback level, the applications are all internal, so the angular measurement experiment should be adjusted for the initial distance to the external cavity in the range $1 < c < 4.6$. A small effect on the SMI signal performance in terms of modulated signal strength. An important direction in the field of SMI applications is the estimation of the value of the laser, since the SMI signal contains information about the value. The above discussion leads to the conclusion that the linewidth spread factor is related to whether the self-mixing interference fringe is tilted, while the optical feedback level factor is related to the degree of tilt of the self-mixing interference fringe.

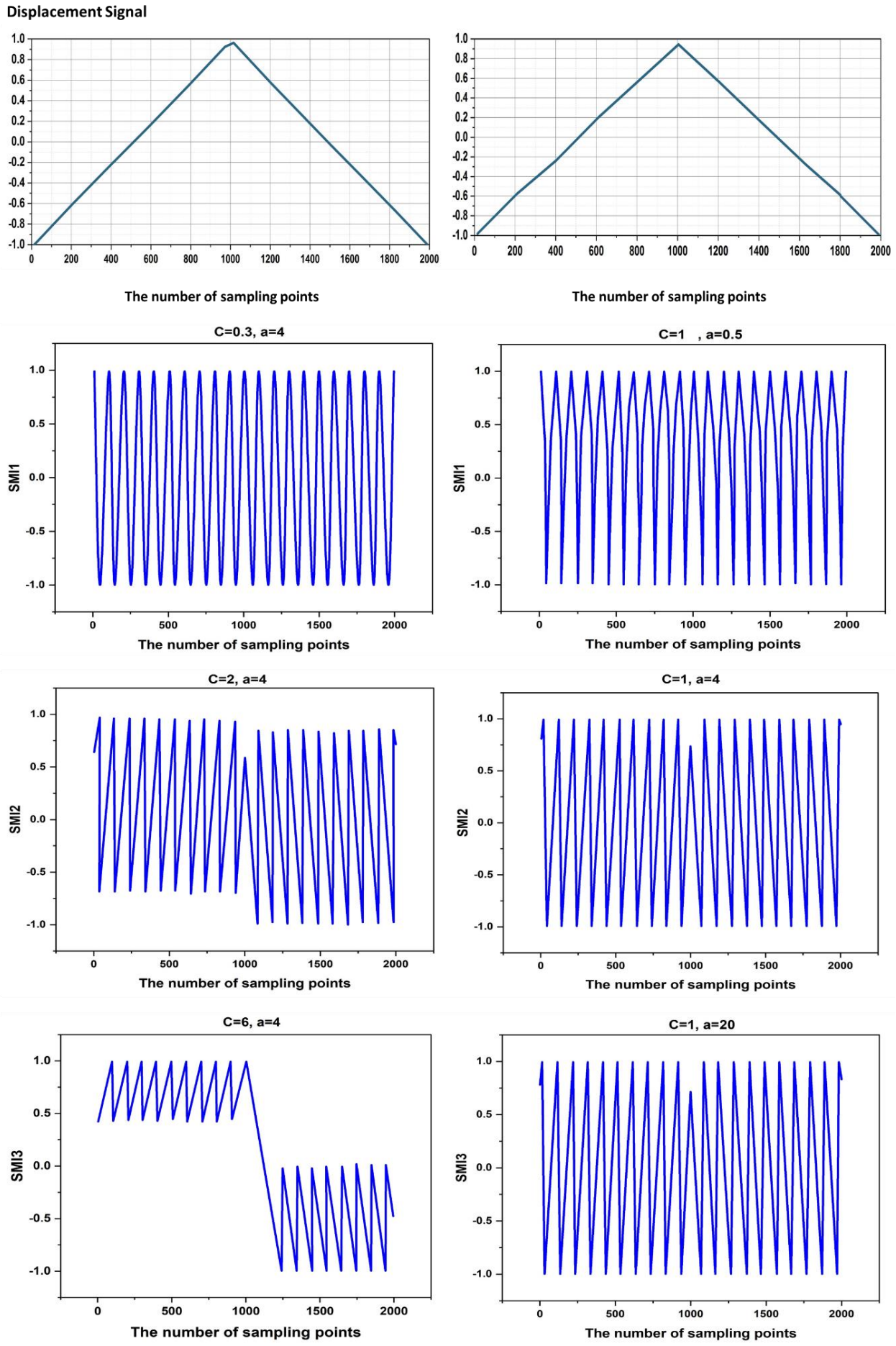

Figure 6. SMI signal at different levels of optical feedback (left) and SMI signal at different line width spreading levels (right)

4. Building an Ultraviolet Optical Communication Channel Estimation System for Mobile Robots

4.1. Software and Hardware Platform for Real-Time Implementation of Channel Estimation for UV Optical Communication

The UV non-line-of-sight communication channel estimation system is an important module of the scattering communication system for UV light. This module consists of a transmitter and receiver system, which in turn consists of their own software and hardware systems. The part of the transmitter side that is related to the channel estimation system is the design of the frame structure, which aims to provide the Barker code sequence for frame synchronization and the Gold training sequence for channel estimation. The parts of the receiver side that are related to the channel estimation system are the signal arrival detection module, the extraction of the frame synchronization signal, and the channel estimation module. The part of the transmitter side that is related to the channel estimation system is the design of the frame structure; this part is to provide the Barker code for frame synchronization and the training sequence for channel estimation. The inclusion of the frame structure creates a data loss problem, which is solved by using different clock frequencies to form the signal. For the incoming data signal, it is first cached into a two-port RAM at a lower clock frequency, and at a higher clock frequency, the frame header and data are carried out to form the baseband signal for the transmit. The design was implemented by an existing FPGA system in the laboratory. The design of the transmitter side is relatively straightforward, as the only part of the channel estimation system that is relevant is the training sequence part of the frame structure, which provides the Barker code for frame synchronization and the training sequence for channel estimation. The receiver side is mainly responsible for the accurate detection of signal arrival, extraction of the synchronization signal, and the completion of the channel estimation using the training sequence, thus enabling the recovery of the signal. The hardware design is as follows.

1. Power Supply Circuit Design

In the C6713 minimal hardware system, the power supply solution uses the DC/DC switching power supply method to obtain 3.3V and 1.26V voltages.

2. Reset Circuit Design (Figure 7)

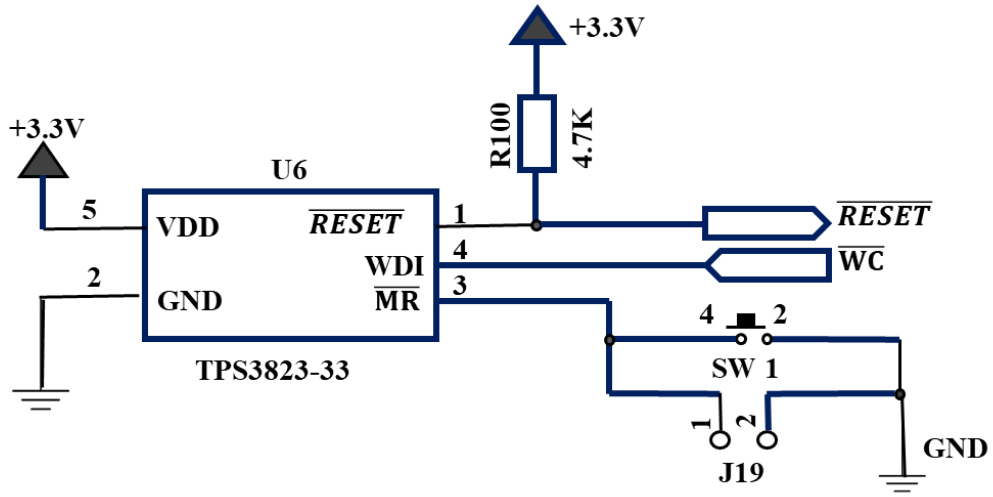

Figure 7. Reset circuit

3. Clock Circuit Design

CKLIN is the C6713 clock source input, CLKMODE0 is set to 0 in this system and CLKIN is selected as the clock source. In the development board, CLKIN is connected to a clock source of 25MHz, and the software generates the required clock signals for the PLL and PLL controller.

The software framework of the UV optical communication channel estimation system consists of a transmitter-side and a receiver-side software framework. The transmitter-side software mainly implements the synchronization signal and training sequence in the data under the FPGA-based platform, while the receiver-side software includes signal arrival detection, data transfer module via C6713EDMA, channel estimation algorithm implemented by interrupt subroutine, and signal recovery algorithm via channel estimation.

4.2. UV Optical Communication Channel Estimation System Implementation

1. Module Design

Firstly, the end frame structure module is designed. A frame header is added to the input data to form a certain format of information frame. The value in ROM is the frame header, which is a fixed constant and is stored in ROM in advance. One of the main tasks of the designed transmitter is to add the frame header to the information code elements. The design of the frame header takes into account two aspects, the training sequence used for equalization and channel estimation, and the frame synchronization code used for frame synchronization. It is concluded that the frame length is 20 times the optimal length of the training sequence, and that the frame header is a total of 200 bits, with the design synchronization code Barker code taking up 13 bits and the Gold training sequence immediately following it actually taking up 187 bits.

Secondly, the design of the signal arrival detection module at the receiver. The purpose of the arrival detection module is to tell the receiver when a useful signal has arrived to start signal processing. The receiver constantly detects the incoming signal and correctly determines whether the signal has arrived or not. According to the frame structure the 13-bit Barker code is designed to be used for signal arrival detection. The transmit signal is and the receive signal is respectively

$$\text{Txsignal} = [\text{bark1}, \text{bark2}, \cdots, \text{bark13}, \text{Pn\_sequnece}, \text{Data}]$$

$$\text{Rxsignal} = [\text{noise}, \text{bark1}', \text{bark2}', \cdots, \text{bark13}', \text{Pn\_sequnece}', \text{Data}']$$

Thirdly, the design of the signal synchronization module at the receiving end. After the arrival of the signal is detected, it is immediately followed by signal synchronization. The synchronization is divided into coarse and fine synchronization, the coarse synchronization being obtained by correlation of the peaks of the pseudo-random sequence. In AWGN channels, coarse synchronization is sufficient. In the case of significant multipath, fine synchronization is required. The specific process of synchronization is that the received pseudo-random sequence is cyclically correlated with the sequence stored in C6713. The maximum correlation value is obtained only when it is exactly aligned; otherwise, the correlation value is small. The received sequence can thus be synchronized at symbol level.

Fourth, the design of the signal estimation algorithm module at the receiver side. The algorithm for implementing the channel estimation can be written using TI's library functions as sub-modules on the one hand, or the channel estimation subroutine in C on the other. The results obtained from the simulation of the UV channel estimation algorithm via MATLAB Simulink are shown in the following two figures, using the NLMS algorithm. Figure 8 shows the MATLAB Simulink simulation graph using this algorithm.

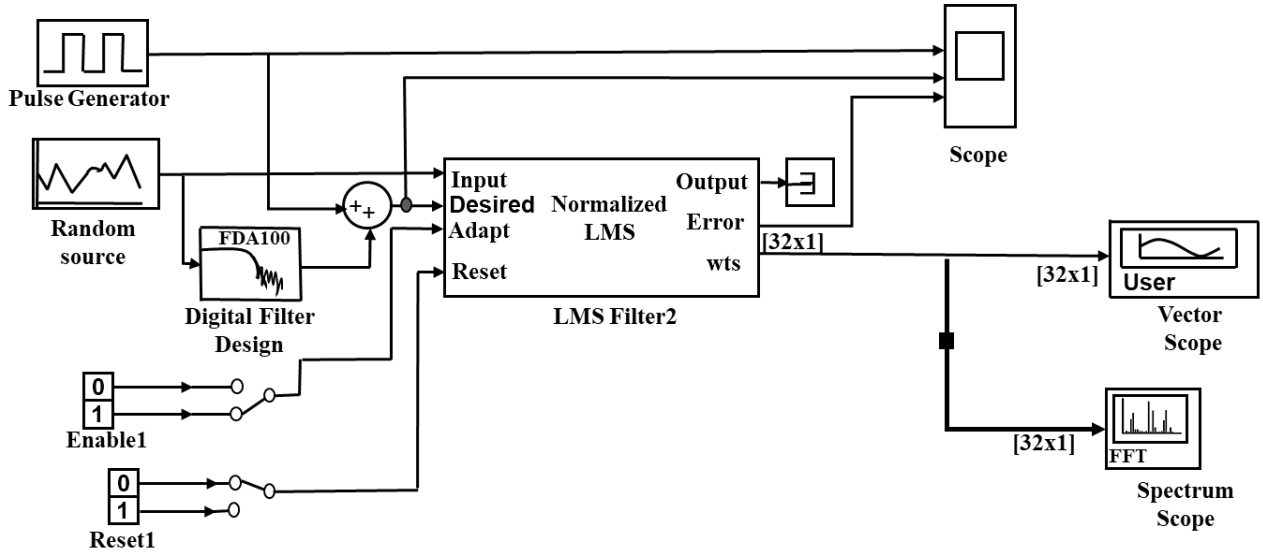

Figure 8. Simulink diagram for UV NLMS channel estimation

2. UV Optical Communication Channel Estimation System Implementation

Firstly, the transmitter side frame structure is implemented. After modulation of the voice encoded signal, the main job is to add a frame header to form a certain format of information frame. The controller provides the write enable signal for the dual-port RAM. The controller has an internal counter which, depending on the count value, generates different control signals to control the readout of the value in the dual-port RAM or ROM. Assuming that the frame header length is l, the values in ROM are read in sequence as the count value goes from 0 to r, with rom _ r being high and ram _ r being low, while the multiplexer also selects ROM, which is the value of the frame header and is fixed and

pre-burned in ROM. When the count value goes from "l + 1" to "L", L being the length of a frame, rom _ r is low and ram _ r is high, the RAM is selected and the message code elements in the dual-port RAM are read out from the low address to the high address. This process is executed cyclically, so that the information frames are continuously output.

Secondly, the DSP implementation of the synchronization module. The arrival of the measured signal is followed by the synchronization of the signal. UV optical communication systems are digital baseband communications, and there is no problem of carrier synchronization, only bit and frame synchronization. Bit-synchronous pulses, or timing pulses, are obtained by means of bit-synchronous extraction circuits. When a digital signal is transmitted, the signal is affected by the noise passing through the channel, which distorts the transmitted waveform. The receiver of a digital communications system must therefore discretize the received baseband signal by sampling it to determine whether it is a code 1 or a code 0. The sampling interval is controlled by the bit-synchronous pulse. The binary clock signal can usually be extracted from the demodulated baseband signal and only in exceptional cases directly from the frequency band signal; the carrier clock signal must be extracted from the frequency band signal. The binary clock in UV optical communication systems can be extracted directly from the baseband signal after leaving the shaping circuit of the photomultiplier. Bit synchronization determines the sampling judgment time for each code element in UV communication, i.e., each code element is differentiated so that the receiver receives a sequence of significant code elements. This sequence of code elements represents a certain amount of information; usually a number of code elements represent a letter, a number of letters form a word, and a number of words form a sentence. When data is transmitted, a certain number of code elements are formed into a code group. The task of image synchronization is to distinguish between words, sentences, or code groups. In UV-optical communication, the frame structure consists of three parts, each with a different number of code elements. The synchronization bit information must be divided by frequency to obtain the pulse frequency of these groups. The frequency of the frame synchronization pulses can be easily obtained from the bit synchronization pulses by dividing the frequencies. The "start" and "end" times of each frame, i.e., the phase of the grouped synchronization pulses, cannot be obtained directly from the synchronization pulses. Determining the "start" and "end" times is an additional problem that must be solved in packet synchronization.

In order to determine the "beginning" and "end" moments of the frame synchronization, a Barker code is added to the frame structure design so that the specific length of the frame structure is known, and the beginning and end moments of the frame structure can be determined using the characteristics of the Barker code. The DSP module is implemented by taking the signal at the time of arrival as the entry parameter, correlating it to obtain the position of maximum energy, and giving the symbol synchronization flag. The beginning and end of the training sequence are determined, the training sequence is extracted and stored in the data memory in preparation for the channel estimation algorithm, and finally the recovery of the data signal is implemented.

The channel estimation algorithm is implemented on the premise that the system accurately detects the arrival of the signal and achieves frame synchronization. The error signal is obtained in the training sequence, from which the channel estimation is achieved under the LMS criterion. After estimating the channel impulse response, the signal is recovered within a certain error range.

5. Construction of a Laser Self-Mixing Interferometric Angle Measurement Device for Mobile Robots

5.1. Design Options for the Measuring Device

The designed laser self-mixing interferometric angle measurement device is based on a three-mirror cavity theoretical model and the stripe counting method combined with geometric calculations for accurate measurement and calculation of the rotating angle. A semiconductor laser is the core component of the optical path design, and a prismatic reflector is attached to both ends of the surface of the object to be measured, which is fixed to a rotating platform and the computer controls the speed and direction of rotation required for the rotating platform. The laser beams emitted by the two semiconductor lasers are incident perpendicularly and parallel to the reflecting prisms, and the incident light is reflected off the prism surface and returned to the laser cavity, where the PD detector converts the light signal into an electrical signal, which is amplified by a signal processing circuit and collected by an oscilloscope for self-mixed interference fringe signals.

The angle measurement device consists of the following modules: laser drive modulation and temperature control module, signal hardware processing module and signal software processing module. The main function of the laser drive modulation is to provide drive and modulation current to the semiconductor laser, the temperature control module allows the laser diode to work in a temperature-controlled environment, ensures that the PD detector receives stable feedback light to form a self-mixed interference signal, and converts the self-mixed interference signal from an optical signal to an electrical signal. The main function of the signal hardware processing module is to amplify the electrical signal transmitted by the PD detector and to collect it by means of an oscilloscope for the subsequent processing of the fringe counting. The software processing module is used by the PC to filter the stripe signal, extract the displacement information of the rotating reflector, differentiate it and count it.

5.2. Device Calibration Design

With the emergence of nano-measurement and metrology requirements in the field of precision measurement, laser self-mixing interference has widely penetrated into the field of precision measurement. The most important means of detection of laser self-mixing interference is the light intensity signal from the laser feedback. As the measurement device ensures that the feedback light is returned to the laser resonance cavity after angular deflection, a self-mixed interference signal with a high signal-to-noise ratio is formed. In laser self-mixing interferometry, the signal-to-noise ratio and accuracy are directly dependent on the stability of the light source. The parallelism of the laser beam is therefore a key part of the overall angle measurement method.

For the spot position detection device, two parallel plates with holes are designed to limit the two laser beams, and two rows of parallel collimated holes are designed based on the principle of geometric parallelism, with the aperture size adjusted and designed according to the beam size, the diameter of the holes being slightly larger than the beam diameter. The two parallel plates are positioned strictly parallel to each other and fixed to the base plate, which is slotted and secured by countersunk holes in the two parallel plates. The mechanical design of the two parallel plates contains a strict parallelism that regulates the passage of the two laser beams through the parallel apertures. The PSD provides information on the position of the beam spot in the detection area and, in conjunction with the parallel plates and the PSD, the double calibration of the beam through the aperture and the PSD allows for better regulation of the parallel vertical light source.

Due to the large amount of measurement data and the fact that the light signal is influenced by the external environment, the parallel plate is designed to be mounted on the same horizontal plane as the PSD position sensor in order to reduce unnecessary errors. In order to better prevent the experimental data from being greatly disturbed by mounting movements, an experimental stand for fixing the parallel plate and the PSD position detector was designed and fabricated and fixed to the rotating platform. The entire test stand is tightly connected, which effectively reduces the interference of external environmental conditions with the measurement experiment, improves the accuracy of the angle measurement device and is more convincing. A diagram of the mechanical structure of the parallel plate device is shown in Figure 9.

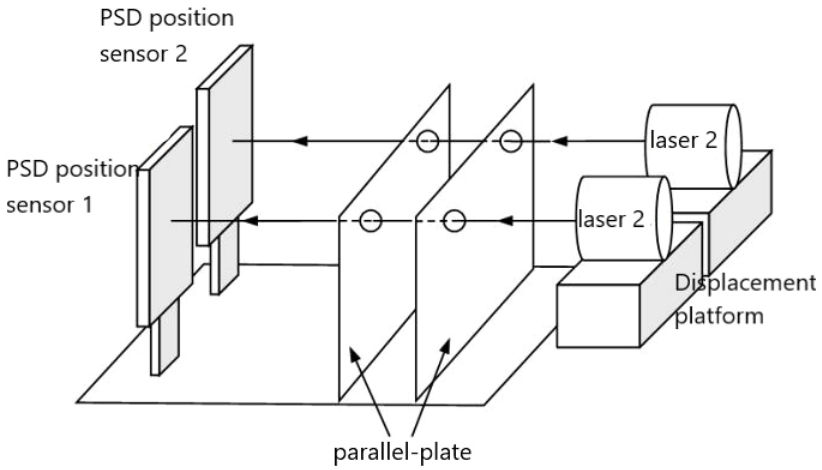

Figure 9. Mechanical structure of the parallel plate device

The laser contains an LD light source, a PD detector and a collimating lens. The laser driver drives the current of the LD light source, which first emits laser light horizontally through the collimating lens, which is fine-tuned to form the light path. The laser attitude is adjusted by means of a high-precision two-dimensional displacement table. The laser beam is passed through a small hole in the parallel plate and, after passing through the hole, the beam is received with a PSD to obtain the beam position deviation. The device is adjusted so that the laser beam passes through the small hole in the parallel plate onto the reflector, and then the position sensor is used to measure the beam position change and get precise feedback on the alignment. The specific design of the PSD, parallel plate etc. is characterized by small and portable size, high measurement accuracy, as well as the technical advantage of monitoring the stability of the measurement beam and fast measurement. This increases the accuracy of the overall device by adding high precision position measurement of the position sensor under overall optical calibration conditions. The addition of a spot detection device to the laser self-mixing interferometric angle measurement technology thus avoids the serious problem of measurement errors caused by deviations of the incident light. The advantage of having an increased parallel collimation

working range at the same working distance, or an increased working distance at the same working range. The provided spot detection device is characterized by simple structure, high adjustment accuracy, constant error in the calibration function and easy operation compared to similar devices in the past for light range adjustment such as interference, ensuring the accuracy of the laser self-mixing angle measurement method.

Using the completed spot position detection device for testing and calibration, two laser beams are passed through parallel holes in the parallel plate to form a spot on the sensitive surface of the PSD, and the two PSDs detect the laser 1 and 2 spot positions respectively. The stability of the spot detection device was tested by simultaneously testing the spot positions of the two laser beams in a powered-up state after the optical path had been collimated. The spot positions were recorded every 5 minutes for 10 consecutive sets of measurements. By analyzing the data results of the PSD test and observing the changes in the spot positions, a phenomenon was observed during the calibration process: the central circular spot was the spot formed by the laser on the PSD detector. This variation causes a slight shift in the position sensor measurement (the amount of shift is probably in the order of microns) and this shift is known as light drift. The reasons for this are analyzed in three ways: drift of the laser light from the laser source itself, slow drift of the light introduced by the adjustment mechanism of the fixed laser and drift of the laser light introduced by air disturbances or uneven distribution of the refractive index.

The light drift eventually causes the laser spot to move back and forth in the most concentrated part, thus affecting the stability of its self-mixed interferometric signal output, and the measurement accuracy is also affected by the light drift. The quality of the beam is critical to the performance of the entire measurement set-up and is therefore calibrated for maximum measurement error due to light drift. In the device, the prism reflector is placed close to the measured surface of the target object and the two laser beams are adjusted to shine parallel to the prism reflector through two small holes in the parallel plate. The fact that the laser beam is not perpendicular to the initial position of the prism reflector during the adjustment process is a major factor in the accuracy of the measurement.

5.3. Construction and Commissioning of the Measuring Device

The angle measurement device is built on an optical platform based on the optical path structure of the laser self-mixing interference effect. In a first step, the parallel collimation device is fixed to a rotating stage and set up on a high precision 2D displacement table, and the lasers 1 and 2 are fixed to the 2D displacement table. Lasers 1 and 2 are connected to the signal hardware processing circuit and the signal is collected by an oscilloscope connected to the BNC interface line on the circuit board. The second step is to lay out the optical path for the parallel collimation of the two beams, using the parallel calibration scheme designed above for the preparation of the beam calibration before the experiment, on the fixed base plate in order to layout, laser 1, laser 2, parallel collimation device, rotating stage, signal processing module, to complete the layout of the self-mixed interference optical path structure. The third step is to use the designed two-way spot position detection device to check whether the beam is parallel collimated. After calibrating the parallel collimated beam, the prismatic reflector is attached to the small hole. At this point the distance between the two prismatic reflectors is known.

The whole device is simpler, more compact and easier to collimate with than conventional optical interferometric systems because it does not require the use of optics such as right-angle prisms or polarizing beam splitters. Fewer optical elements and therefore less space is required for angle measurement.

6. Results

In mobile robotics, Non-Line-of-Sight Optical Communication Signal Processing utilizes Laser Self-Mixing Interference to enable sensing measurements. The results show enhanced capabilities for diverse sensing tasks, including obstacle detection and localization, leveraging intricate optical phenomena. This innovation promises robustness and performance in challenging environments for mobile robotic systems. SNR and robotic localization performance are used for these results. Distance, velocity, object shape are the sensing measurements utilizing for SNR and laser range finder, camera, light detection and ranging (LiDAR) are the sensing modality employing for robotic localization performance.

Signal-to-Noise Ratio (SNR): SNR in mobile robotics, particularly in non-line-of-sight optical communication with laser self-mixing interference effects, reflects the quality of sensing measurements by comparing the strength of the desired signal to background noise. SNR indicates clearer, more reliable data amidst challenging environmental conditions, crucial for accurate robotic operations. The SNR values are represented in decibels (dB). Table 1 and Figure 10 shows the SNR values outcomes. The achieved SNR values are Distance (15 dB), velocity (12 dB), and object shape (18 dB).

Table 1. Numerical outcomes of SNR

Sensing Measurement	SNR (dB)
Distance	15
Velocity	12
Object shape	18

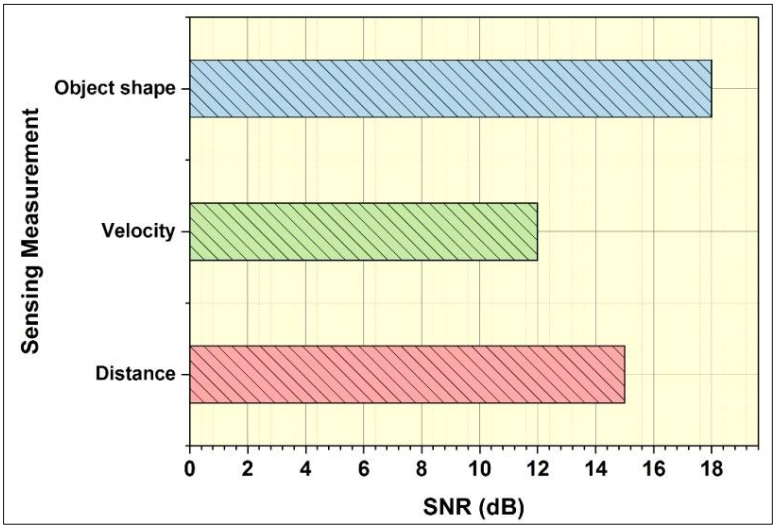

Figure 10. Graphical representation of SNR

***Robotic Localization Performance*:** Robotic localization performance in mobile robotics, using non-line-of-sight optical communication signal processing with laser self-mixing interference effects, varies based on sensing measurements. This approach integrates laser self-mixing interference to enhance localization accuracy. The system's effectiveness hinges on optimizing signal processing algorithms to interpret the interference patterns, enabling reliable localization even in challenging environments with obstructed line-of-sight conditions. The SNR values are represented in centimeters (cm). Table 2 and Figure 11 show the robotic localization performance values outcomes. The obtained robotic localization performances are laser range finder (5 cm), camera (15 cm), and LiDAR (3 cm).

Table 2. Numerical outcomes of robotic localization performance

Sensing Modality	Localization Performance (cm)
Laser Range Finder	5
Camera	15
LiDAR	3

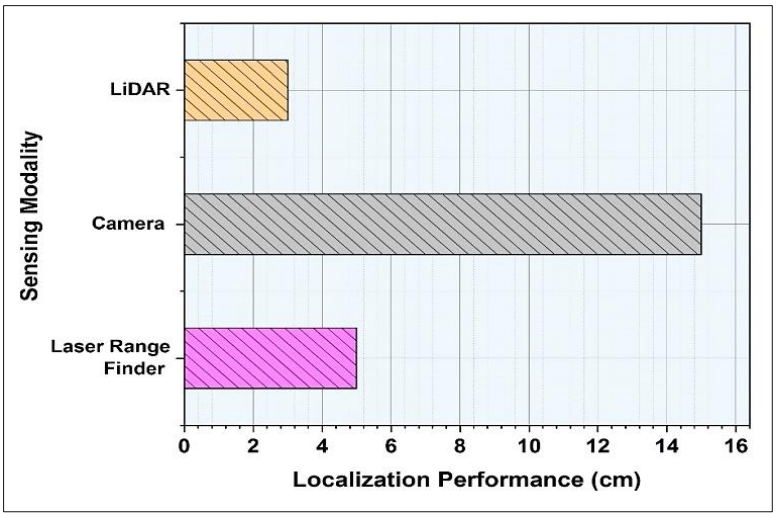

Figure 11. Graphical representation of robotic localization performance

7. Conclusion

Mobile robotics in non-line-of-sight optical communication utilizes laser self-mixing interference for diverse sensing measurements, employing signal processing techniques to interpret data for navigation and environmental perception in dynamic environments. In this paper, the UV single scattering model establishes a transmission model for the UV signal, obtains approximate results for the channel impulse response, simulates the length of the channel impulse response, and simulates the relationship between the channel impulse response and the transmit-receive geometry and setup in order to investigate the various sensing measurements of mobile robotics in non-line-of-sight optical communication signal processing with laser self-mixing interference effects. The path loss is simulated for a variety of scenarios. The overall structure of the angle measurement device and elaborates on the design process and design principles of the spot position detection device. The spot position is detected by a PSD position sensor, the parallelism of the beam is calibrated, and the spot positions of the two light sources are compared, and the causes of the drift phenomenon are investigated. SNR and robotic localization performance are used for these results. Distance, velocity, and object shape are the sensing measurements utilized for SNR. Laser range finders, cameras, and light detection and ranging (LiDAR) are the sensing modalities utilized for robotic localization performance. Distance (15 dB), velocity (12 dB), and object shape (18 dB) in SNR. Laser range finder (5 cm), camera (15 cm), and LiDAR (3 cm) in robotic localization performance. Limitations include potential inaccuracies due to environmental factors, limited range, and challenges in real-time implementation and calibration. Future work could explore laser self-mixing interference for mobile robotics, enhancing non-line-of-sight optical communication for diverse sensing applications through signal processing advancements.

8. Declarations

8.1. Author Contributions

Conceptualization, S.L. and C.G.; methodology, S.L.; software, S.L.; validation, S.L. and C.G.; formal analysis, C.G.; investigation, S.L.; resources, C.G.; data curation, C.G.; writing—original draft preparation, C.G.; writing—review and editing, S.L.; visualization, S.L.; supervision, C.G.; project administration, C.G.; funding acquisition, S.L. All authors have read and agreed to the published version of the manuscript.

8.2. Data Availability Statement

The data presented in this study are available on request from the corresponding author.

8.3. Funding

1) 2022 industry-academia cooperation and collaborative education project of the ministry of education: "Construction of practice base based on application-oriented talent training. (fund no.: 220505181032338)";

2) Jilin province higher education scientific research topics: "Research on talent training system of software engineering in universities facing wisdom education";

3) Teaching reform project: "Research and practice on high quality development of higher education in Jilin province from the perspective of strong province of education".

8.4. Institutional Review Board Statement

Not applicable.

8.5. Informed Consent Statement

Not applicable.

8.6. Declaration of Competing Interest

The authors declare that they have no known competing financial interests or personal relationships that could have appeared to influence the work reported in this paper.

9. References

[1] Li, W., Zhou, Y., Du, W., Peng, Y., & Li, J. (2021, April). Application of the precision industrial measurement technology in geometric measurement. IOP Publishing: Journal of Physics: Conference Series, 1885 (2), 022021. doi:10.1088/1742-6596/1885/2/022021.

[2] Tao, C., Wu, Y., Wang, W., Qian, Y., Tao, R., & Kang, T. (2019). Experimental investigation of white-light interferometry based on sub-dark-field illumination. Optics Communications, 435, 108-117. doi:10.1016/j.optcom.2018.11.020.

[3] Huang, Z., Nie, Z., Xu, H., Zhao, S., Chen, G., Hu, X., ... & Li, D. (2024). A Multilongitudinal Mode Quadrature Laser Self-Mixing Vibration Sensor for Fault Diagnosis of Bearing. IEEE Sensors Journal, 24(4), 4407-4417. doi:10.1109/JSEN.2023.3348143.

[4] Hu, L., & Dai, S. (2022). Nano-semiconductor materials. Dye-sensitized Solar Cells, 7, 41. doi:10.1515/9783110344363.

[5] Zhang, P. C., & Xu, D. (2015). Tracking and guiding multiple Laser beams for beam and target alignment. International Journal of Automation and Computing, 12(6), 600-610. doi:10.1007/s11633-015-0908-8.

[6] Chen, L., Zhang, D., Zhou, Y., Liu, C., & Che, S. (2018). Design of a high-precision and non-contact dynamic angular displacement measurement with dual-Laser Doppler Vibrometers. Scientific Reports, 8(1), 9094. doi:10.1038/s41598-018-27410-4.

[7] Wang, K., Chen, Q., Jiang, C., Chen, Z., Lou, J., Lu, M., ... & Guo, W. (2023). Characterization of thermo-optically tuned multi-channel interference widely tunable semiconductor laser for quasi-continuous tuning. Journal of Lightwave Technology, 41(10), 3084-3093. doi:10.1109/JLT.2023.3241892.

[8] Duan, Y., Liang, L., Tong, X., Luo, B., & Cheng, B. (2023). Application of pipeline leakage detection based on distributed optical fiber acoustic sensor system and convolutional neural network. Journal of Physics D: Applied Physics, 57(10), 105102. doi:10.1088/1361-6463/ad1144.

[9] Wu, J., Chen, Y., Guo, R., & Chen, J. (2024). A dynamic turbine tip clearance measurement method based on laser self-mixing interferometric ranging considering Doppler effect. Measurement Science and Technology, 35(11), 115012. doi:10.1088/1361-6501/ad6a75.

[10] Chen, H., Zhong, Z., Ge, S., Zhu, D., Lin, Y., Kong, X., ... & Huang, W. (2024). Robust Time-Domain-Based Spectral Processing Method for Laser Self-Mixing Vibration Measurement. IEEE Transactions on Instrumentation Measurement, 73, 3449962. doi:10.1109/TIM.2024.3449962.

[11] Lin, F., Ali, M., Tan, Y., Su, Z., & Wong, H. (2023). Laser offline measurement method based on self-mixing interference for thin-wall fused deposition modelling component. Journal of Manufacturing Processes, 102, 131-142. doi:10.1016/j.jmapro.2023.07.041.

[12] Zhao, S., Xin, H., Wu, S., Sun, Y., & Hu, B. (2024). Attenuation of Ultraviolet Radiation by Aerosols and Clouds in Beijing Area in 2005–2020. Atmosphere, 15(3), 311. doi:10.3390/atmos15030311.

[13] Shan, T., Yuan, R., He, N., & Cheng, J. (2023). Non-line-of-sight ultraviolet transmission coverage in non-precipitating, foggy, and rainy weather. Optics Express, 31(23), 37703-37721. doi:10.1364/OE.502380.

[14] Wang, P., Xiang, X., Dong, P., & Liang, Y. (2024). Maximum Likelihood Sequence Estimation Optimum Receiver Design with Channel Identification Based on Zero Distribution. Electronics, 13(19), 3877. doi:10.1109/COMST.2023.3339371.

[15] Mustafa, R., Sarkar, N. I., Mohaghegh, M., & Pervez, S. (2024). A Cross-Layer Secure and Energy-Efficient Framework for the Internet of Things: A Comprehensive Survey. Sensors (Switzerland), 24(22), 7209. doi:10.3390/s24227209.

[16] Liu, X., Lu, H., Zhu, Y., Ma, J., Hao, R., Chen, D., & Wang, J. (2024). Experimental study on the transmission performance of an ultraviolet and visible light communication system under an artificial fog channel. Optics Express, 32(17), 30622-30631. doi:10.1364/OE.525762.

[17] Kannapiran, S., Chandran, S., Jayasuriya, S., & Berman, S. (2024). PathFinder: Attention-Driven Dynamic Non-Line-of-Sight Tracking with a Mobile Robot. arXiv preprint, arXiv:2404.05024. doi:10.48550/arXiv.2404.05024.

[18] Zhao, Y., Zhang, B., & Han, L. (2020). Laser self-mixing interference displacement measurement based on VMD and phase unwrapping. Optics Communications, 456, 124588 2020. doi:10.1016/j.optcom.2019.124588.

[19] Sun, W., Yang, Z., Feng, G., Chen, Z., Chang, Q., Hai, L., & Guo, Z. (2023). A Novel Method for Detecting Fe2+ at a Micromolar Concentration Based on Multiple Self-Mixing Interference Using a Fiber Laser. Sensors, 23(5), 2838 2023. doi:10.3390/s23052838.

[20] Liu, H., You, Y., Li, S., He, D., Sun, J., Wang, J., & Hou, D. (2023). Denoising of Laser Self-Mixing Interference by Improved Wavelet Threshold for High Performance of Displacement Reconstruction. Photonics, 10(8), 943. doi:10.3390/photonics10080943.

[21] Wang, X., Zhong, Z., Chen, H., Zhu, D., Zheng, T., & Huang, W. (2023). High-Precision Laser Self-Mixing Displacement Sensor Based on Orthogonal Signal Phase Multiplication Technique. Photonics, 10(5), 575. doi:10.3390/photonics10050575.

[22] Yu, L., Yang, Y., Liu, B., Tang, P., Ji, H., Wang, J., & Tan, T. (2023). Laser Self-Mixing Interference: Optical Fiber Coil Sensors for Acoustic Emission Detection. Photonics, 10(9), 958. doi:10.3390/photonics10090958.

[23] Shen, E., Duan, S., Guo, S., & Yang, W. (2024). Object Localization and Sensing in Non-Line-of-Sight Using RFID Tag Matrices. Electronics (Switzerland), 13(2), 341 2024. doi:10.3390/electronics13020341.

[24] Liu, B., Wang, B., Ruan, Y., Yu, Y., Xi, J., Ji, H., & Tang, P. (2024). Time-multiplexed laser self-mixing sensor for measurement of multiple material elastic moduli. Optics and Laser Technology, 176, 110963 2024. doi:10.1016/j.optlastec.2024.110963.

[25] Zhao, Y., & Zhang, H. (2021). Angle measurement method based on speckle affected laser self-mixing interference signal. Optics Communications, 482, 126569 2021. doi:10.1016/j.optcom.2020.126569.

[26] Zhao, T., Li, Y., & Yuan, L. (2019). Research on relay selection of armored formations wireless UV covert communication. Opto-Electronic Engineering, 46(5), 180448. doi:10.12086/oee.2019.180448.

[27] Yue, K. (2024). Application of EEUC-based inter aircraft ultraviolet communication network algorithm in energy consumption optimization of drone swarm. Energy Informatics, 7(1), 27. doi:10.1186/s42162-024-00331-5.

[28] Zhao, T., Cheng, M., Lyu, X., Zhang, H., & Wang, L. (2024). An unequal clustering energy consumption balancing routing algorithm of UAV swarm based on ultraviolet secret communication. Wireless Personal Communications, 137(1), 221-235. doi:10.1007/s11277-024-11394-8.